Microscale simulation of terrain-disrupted airflow around the Hong Kong International Airport (HKIA) – comparison of results between numerical models

P.W. Chan *
Hong Kong Observatory, Hong Kong, China

T.C. Cheung
Chinese University of Hong Kong, Hong Kong, China

1. INTRODUCTION

The Hong Kong International Airport (HKIA) is situated in an area of complex terrain. To its south is the mountainous Lantau Island with peaks rising to about 1000 m AMSL with valleys as low as 400 m in between. Terrain-disrupted airflow could occur over and around HKIA when the prevailing winds are from east to southwest, in particular when strong east to southeasterly winds blow over the airport in the spring under a stable boundary layer, and when intense southwest monsoon affects the region in the summer. The airflow disturbances may be hazardous to the aircraft landing at and departing from HKIA, leading to low-level windshear and turbulence.

Observation and forecasting of terrain-disrupted airflow would be crucial in the assurance of aviation safety. On the observation side, two Doppler LIDAR systems are operated inside HKIA because the significant airflow disturbances mostly occur in clear-air conditions. Emitting a laser beam with a wavelength of about 2 microns, the LIDAR scans over the airport area and gives the general wind distribution, though only the line-of-sight velocity is measured. Further technical details and the applications of the LIDAR at HKIA could be found in Shun and Chan (2008). Moreover, a couple of boundary-layer radar wind profilers are operated near the airport. They emit radio waves with a frequency of 1299 MHz vertically into the sky and track the motion of the reflectivity inhomogeneity in the atmosphere in the determination of the three components of the wind. The vertical velocity output from the wind profiler could be useful in the detection of wavy motion as the air climbs over the mountains on Lantau Island.

On the forecasting side, the use of high resolution numerical modelling of terrain-disrupted airflow at HKIA has been attempted. For instance, in Chan (2009), the Regional Atmospheric Modelling System (RAMS) version 6.0 was used with different turbulence parameterization schemes. It turned out that the main features of terrain-induced airflow disturbances in selected events in the spring and summer could be reproduced successfully in the simulations. The model-forecast turbulence intensity also compared reasonably well with the actual observations from the LIDAR and radar wind profilers.

In this paper, the capability of Weather Reserch and Forecasting (WRF) model version 2.2 in the simulation of terrain-disrupted airflow near HKIA is studied. High resolution simulations are made, namely, with a spatial resolution of several hundred metres. The simulation results are compared with those from RAMS to evaluate the performance of the two models. This paper is organized as follows. Section 2 deals with the model setup. Two case studies are presented in Sections 3 and 4. Conclusions are drawn in Section 5.

2. MODEL SETUP

WRF version 2.2 and RAMS version 4.4 are used in the present study for high-resolution simulations. They are nested with the operational regional spectral model of the Hong Kong Observatory (HKO) at a spatial resolution of 20 km. Three nested runs are then performed with WRF and RAMS, namely, at a resolution of 4 km, 800 m and 200 m (Grids 1 to 3). The WRF domains for the first two nested runs are shown in Figure 1. The RAMS domains of these two runs are similar (not shown). The third domains of WRF and RAMS are depicted in Figures 2(a) and (b) respectively. In all model runs, there are no assimilation of actual observations. Only the outer model is used to drive WRF and RAMS through the initial and boundary conditions.

For the topography, Grid 1 uses the 30 arc-second Advanced Very High Resolution Radiometer (AVHRR) dataset from U.S. Geological Survey. In order to resolve the major terrain features near HKIA, high resolution terrain data are employed in Grids 2 and 3, namely, the 3 arc-second resolution data from Shuttle Radar Topography Mission (SRTM).

The model physics options used in the WRF simulation include: WRF single moment 5-class (WSM5) scheme for microphysics, rapid radiative transfer model (RRTM) for longwave radiation, MM5 (Dudhia) scheme for shortwave radiation, Monin-Obukhov scheme for surface layer, cumulus parameterization switched off, and Mellor-Yamada-Janjic (MYJ) turbulent kinetic energy (TKE) scheme.

In RAMS, the corresponding physics options are as follows. The microphysical processes represented in the model include nucleation, evaporation, sublimation, freezing, melting, hydrometer collisions, etc. The shortwave and longwave radiation schemes consider cloud effects in calculating the heating and cooling caused by radiative flux divergence. Convective parameterization is not activated. Turbulence is parameterized as a prognostic TKE equation of Mellor and Yamada scheme.

* *Corresponding author address:* P.W. Chan, Hong Kong Observatory, 134A Nathan Road, Hong Kong
email: pwchan@hko.gov.hk

3. SPRING-TIME EASTERLY WIND CASE

A typical case of spring-time terrain-disrupted airflow near HKIA on 8 March 2006 is considered. Synoptically, a ridge of high pressure over southeastern coast of China brought a fresh to strong easterly airstream to the south China coast. From the 00 UTC radiosonde ascent on that day, there was a temperature inversion of a couple of degrees between 300 and 700 m AMSL. The east to southeasterly airstream together with the stable boundary layer favour the occurrence of terrain-induced airflow disturbances over and around HKIA as the winds climb over the mountains of Lantau Island.

The Doppler velocity imagery from the horizontal conical scan of the LIDAR at HKIA (at about 50 m AMSL) is shown in Figure 2(e). There was an east to southeasterly jet of about 11 m/s to the northwest of the airport. At the same time, an area of reverse wind direction (coloured green in Figure 2(e)) was observed off the northwestern coast of Lantau Island. This area of opposite wind direction (compared to the prevailing east to southeasterly winds) and weaker airflow is believed to arise from the wake associated with the mountains on Lantau Island, which are higher than the temperature inversion as shown in the radiosonde ascent data.

Both the WRF and RAMS simulations in the innermost domain could successfully reproduce this mountain wake. They are shown in Figures 2(a) and 2(b) respectively. The models are initialized at 00 UTC, 8 March 2006 and the simulation results after one hour are shown. The features of terrain-disrupted airflow are observed to have fully developed in the model simulations and they persist for a couple of more hours (not shown). The WRF simulation appears to be better in capturing the mountain wake, namely, a wake with less extensive area in comparison with RAMS simulation. This is more consistent with the actual LIDAR observations. A more accurate forecast of the size of the mountain wake would be helpful, for instance, in the assessment of the occurrence and strength of low-level windshear to be encountered by the aircraft landing at the airport from the west.

In order to see if the differences in the simulation results are related to the treatment of the background temperature profiles, the vertical temperature distributions in WRF and RAMS forecasts at a point far upstream of Lantau Island are shown in Figures 2(c) and 2(d) respectively. It appears that the main features of the two temperature profiles within the boundary layer are very similar. Therefore, the differences in the forecasts between the two model runs may be related to the different numerical implementation of the physical processes inside the models. A more detailed analysis would be required in this aspect.

It is also noted that the two models do not capture the low-level southeasterly jet of about 11 m/s very well. In reality, the jet occurred to the northwest of the airport (coloured orange in Figure 2(e)). WRF simulation successfully forecasts a jet, but it is located to the west of the airport (Figure 2(a)). On the other hand, such a jet is far much less in spatial extent in the RAMS simulation (Figure 2(b)).

Apart from the horizontal wind distribution, the vertical air motion in the model simulations is also compared with the actual observation. The vertical wind data from Siu Ho Wan wind profiler (location in Figure 2(e)) are considered. The vertical velocity distributions in WRF and RAMS simulations are given in Figures 3(a) and 3(b) respectively. They both show that there is a train of mountain wave downstream of the hills near Siu Ho Wan. The wave extends to one wavelength in WRF simulation, but up to two wavelengths in RAMS simulation. As such, downward motion is expected at Siu Ho Wan in WRF forecast, but not in RAMS forecast. Compared with the actual wind profiler data at that time (Figure 3(c)), it appears that WRF simulation is more reasonable.

4. SOUTHWESTERLY FLOW CASE

To consider another wind regime, the strong southwesterly flow on 19 April 2008 is considered. On that day, Typhoon Neoguri over inland areas of Guangdong brought gale-force southwesterly winds to the coast of southern China. The velocity imagery from the 3.2-degree conical scan (elevation angle with respect to the horizon) of the LIDAR inside HKIA (but at a different location compared with the previous case) is shown in Figure 4(c). South to southwesterly winds of 22 m/s were observed. Overall the wind pattern around HKIA was not uniform due to gustiness of the winds associated with a tropical cyclone and the disruption of the airflow by Lantau terrain.

The models are initialized at 06 UTC, 19 April 2008. The forecasts of WRF and RAMS at 14:30 UTC on that day are shown in Figures 4(a) and 4(b) respectively. In general, WRF simulation successfully captures the high-speed wind streaks and blobs (which may be gusty winds arising from terrain disruption of the prevailing flow) in the south to southwesterly airflow, though the westerly component of the winds is too large in the simulated wind field. On the other hand, RAMS forecasts a too rapid decay of the winds following the landfall of the tropical cyclone and, overall speaking, the winds are weaker and more uniform over the airport area in comparison with the actual LIDAR observations.

5. CONCLUSIONS

Microscale simulations are performed using WRF and RAMS with a spatial resolution down to 200 m near HKIA to study terrain-induced airflow disturbances. Both models appear to have skills in forecasting the complex wind patterns. In particular, WRF appears to perform better in capturing the areal extent of the mountain wake in a stable boundary layer in the spring time and the wind-speed wind streaks associated with the southwesterly flow of a tropical cyclone. However, the present study considers just two selected cases, and simulations for more cases of terrain-disrupted airflow would be required in order to find out which model is better in the treatment of the physical processes in microscale.

References

Chan, P.W., 2009: Atmospheric turbulence in complex terrain: verifying numerical model results with observations by remote-sensing instruments. *Meteorology and Atmospheric Physics*, **103**, 145–157.

Shun, C.M., and P.W. Chan, 2008: Applications of an infrared Doppler Lidar in detection of wind shear. *Journal of Atmospheric and Oceanic Technology*, **25**, 637 – 655.

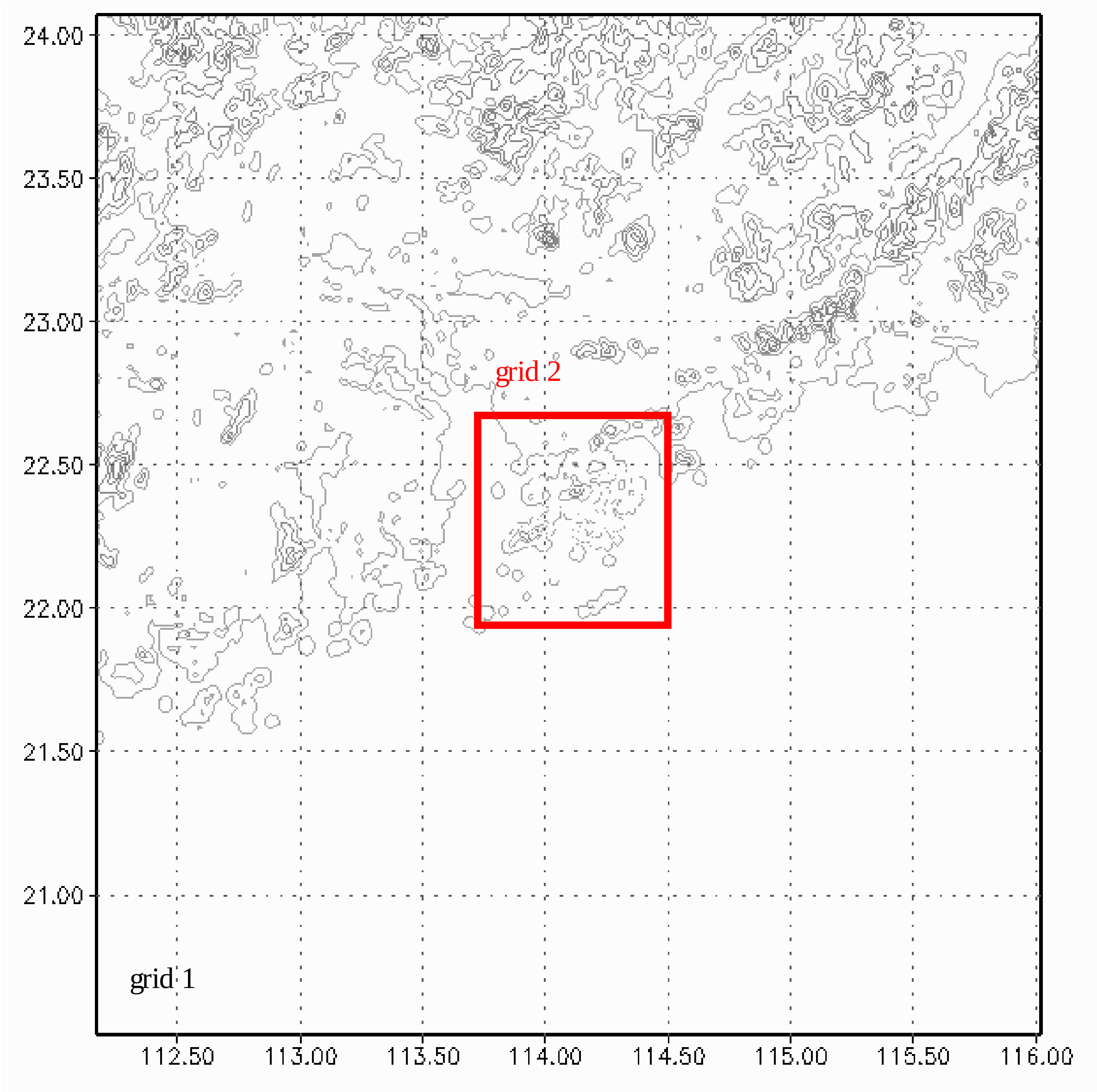

Figure 1 Model domains for grids 1 and 2 in the WRF and RAMS simulations.

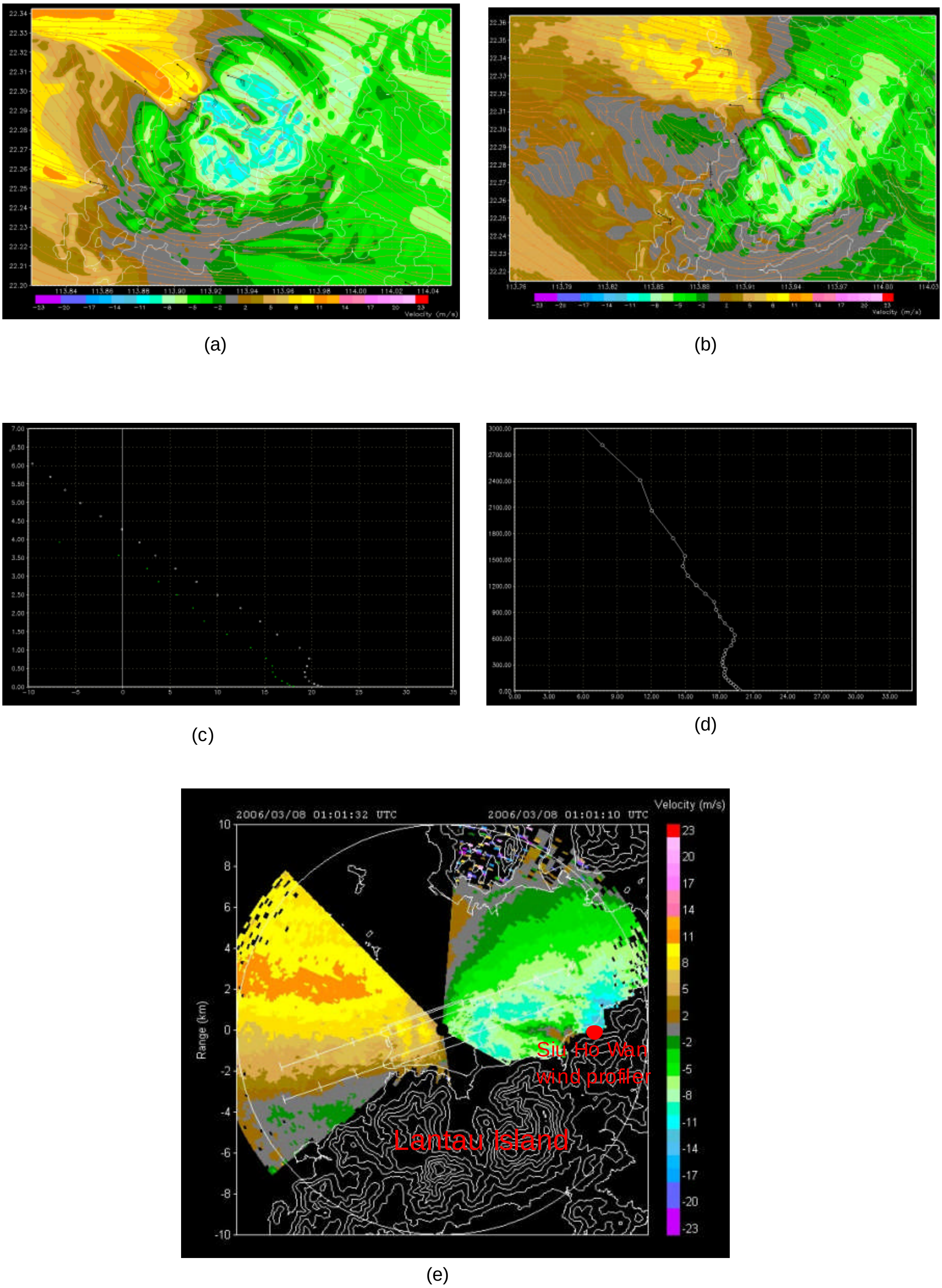

Figure 2 The simulated radial velocity field at 50 m AMSL from (a) WRF and (b) RAMS at 01 UTC, 8 March 2006. The vertical temperature profile at a location upstream of Lantau Island for (c) WRF and (d) RAMS is shown as white points/graph (the green points in (c) are the dew point values). The actual LIDAR observations of radial velocity at the same time are shown in (e).

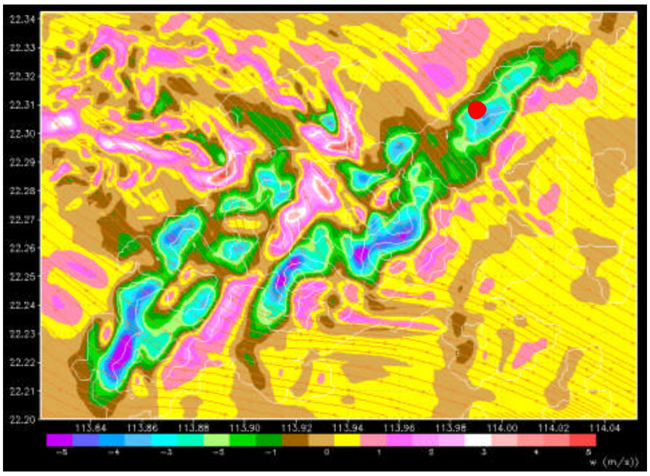

(a)

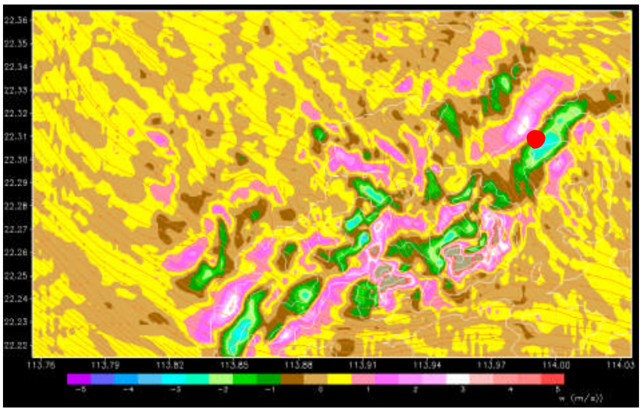

(b)

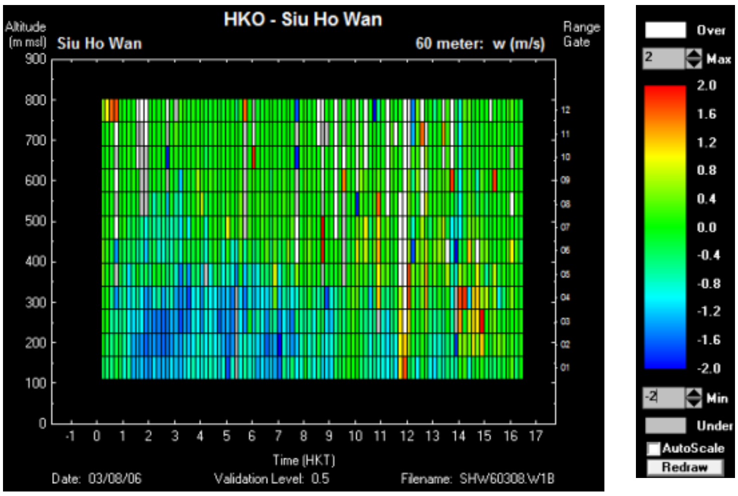

(c)

Figure 3 The simulated vertical velocity field at about 300 m AMSL from (a) WRF and (b) RAMS at 01 UTC, 8 March 2006. The actual vertical velocity measurements from the wind profiler at Siu Ho Wan on that day are given in (c) (in Hong Kong time = UTC + 8 hours). Location of the Siu Ho Wan wind profiler is shown as a red dot in (a) and (b).

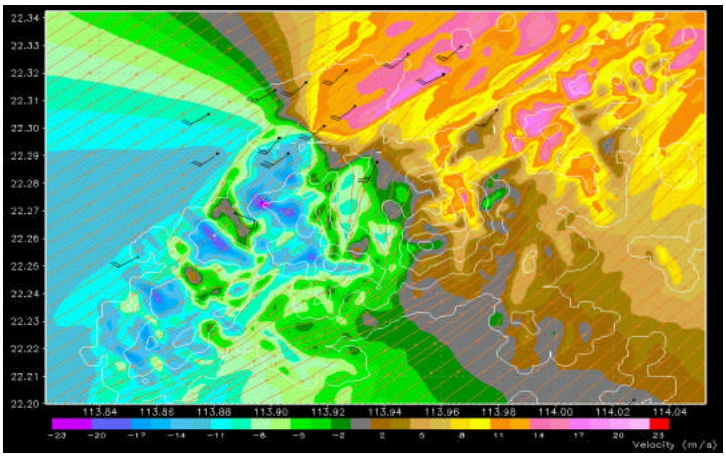

(a)

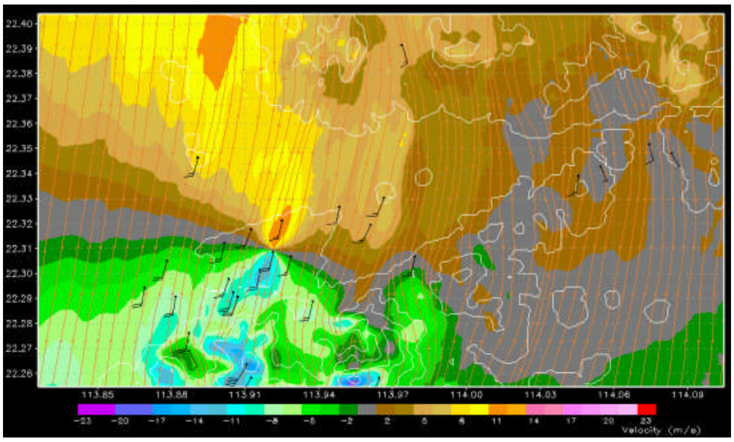

(b)

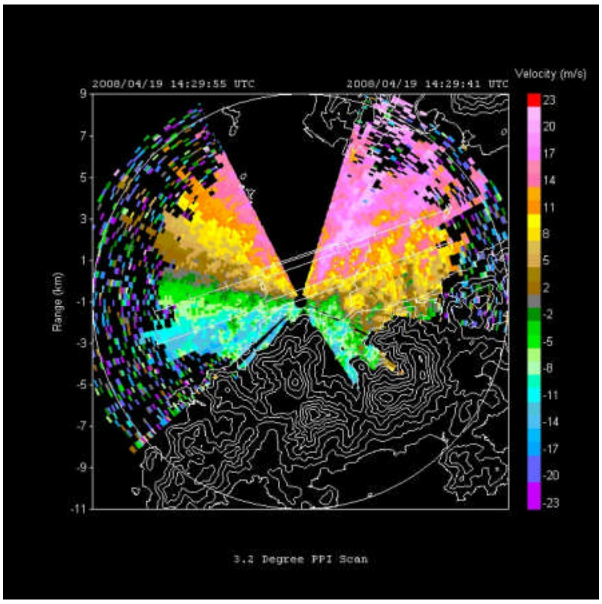

(c)

Figure 4 The simulated radial velocity field at about 100 m AMSL from (a) WRF and (b) RAMS at 14:30 UTC, 19 April 2008. The actual radial velocity measurements from the LIDAR in 3.2-degree conical scan at that time are shown in (c).